Dynamical Control of Nuclear Isomer Depletion via Electron Vortex Beams

Yuanbin Wu[,1,*] Simone Gargiulo[,2] Fabrizio Carbone,[2] Christoph H. Keitel[,1] and Adriana Pálffy[1,3,†]

[1]*Max-Planck-Institut für Kernphysik, Saupfercheckweg 1, D-69117 Heidelberg, Germany*
[2]*Institute of Physics, Laboratory for Ultrafast Microscopy and Electron Scattering,*
École Polytechnique Fédérale de Lausanne, Station 6, Lausanne 1015, Switzerland
[3]*Department of Physics, Friedrich-Alexander-Universität Erlangen-Nürnberg, D-91058 Erlangen, Germany*

Some nuclear isomers are known to store a large amount of energy over long periods of time, with a very high energy-to-mass ratio. Here, we describe a protocol to achieve the external control of the isomeric nuclear decay by using electron vortex beams whose wave function has been especially designed and reshaped on demand. Recombination of these electrons into the isomer's atomic shell can lead to the controlled release of the stored nuclear energy. On the example of ^{93m}Mo, we show theoretically that the use of tailored electron vortex beams increases the depletion by 4 orders of magnitude compared to the spontaneous nuclear decay of the isomer. Furthermore, specific orbitals can sustain an enhancement of the recombination cross section for vortex electron beams by as much as 6 orders of magnitude, providing a handle for manipulating the capture mechanism. These findings open new prospects for controlling the interplay between atomic and nuclear degrees of freedom, with potential energy-related and high-energy radiation source applications.

Nuclear isomers are metastable, long-lived excited states of atomic nuclei. Their direct decay to lower-lying levels is strongly suppressed, typically due to large differences in either spin, nuclear shape, or spin projection on the nuclear symmetry axis [1,2]. In some nuclei with an advantageous level configuration, an excitation to a level above the isomeric state (termed gateway state) can lead to decay directly to a level below the isomer itself, thus reaching the ground state in a fast cascade in a process called isomer depletion. A typical example is the case of the 2425 keV ^{93m}Mo isomer with a half life of 6.8 h, for which we present the relevant partial level scheme in Fig. 1. A 4.85 keV excitation from the isomer to the gateway state at 2430 keV [3] should release the entire stored energy within only 4 ns. Isomer depletion has often been mentioned in the context of potential nuclear energy storage solutions without involving fission or fusion [1,4–6].

One of the most intriguing means to externally drive the transition to the gateway state is via coupling to the atomic shell. In the process of nuclear excitation by electron capture (NEEC), an electron recombining into an atomic vacancy of an ion transfers resonantly its energy

to the nucleus. The sum of the free electron energy and capture orbital binding energy must thereby match, within the uncertainty relations, the nuclear transition energy. This process, originally predicted in 1976 [7], attracted a number of theoretical studies [8–12] prior to the first claim of experimental observation in ^{93}Mo [6]. As theoretical works contradict the experimental results [13,14], the subject is at present a matter of vivid debate [15,16]. Controversy aside, the overall consensus is that, due to the small nuclear transition energy to the gateway state of ^{93m}Mo, NEEC should be stronger than photoexcitation.

So far, the NEEC process has been considered for the case of plane wave electrons captured by ions that are initially in their electronic ground state. However, few recent works suggested that the NEEC cross section can be influenced by the ion's out of equilibrium conditions [17,18] or a different shape of the electronic wave function [19]. In this Letter, we take an important step to investigate the process of NEEC considering specially designed electron vortex beams, which are tailored to enhance the nuclear excitation. Electron vortex beams carry both orbital angular momentum about their beam axis and the electron's intrinsic spin momentum. The angular momentum aspect is particularly important for nuclear transitions that display in the low-energy region mostly a dipole-forbidden character. Our results show that capturing an electron with a properly reshaped wave function can lead to an increase of the NEEC cross section by a few orders of magnitude, depending on the specific situation considered. Furthermore, by manipulating the wave function of the incident electronic
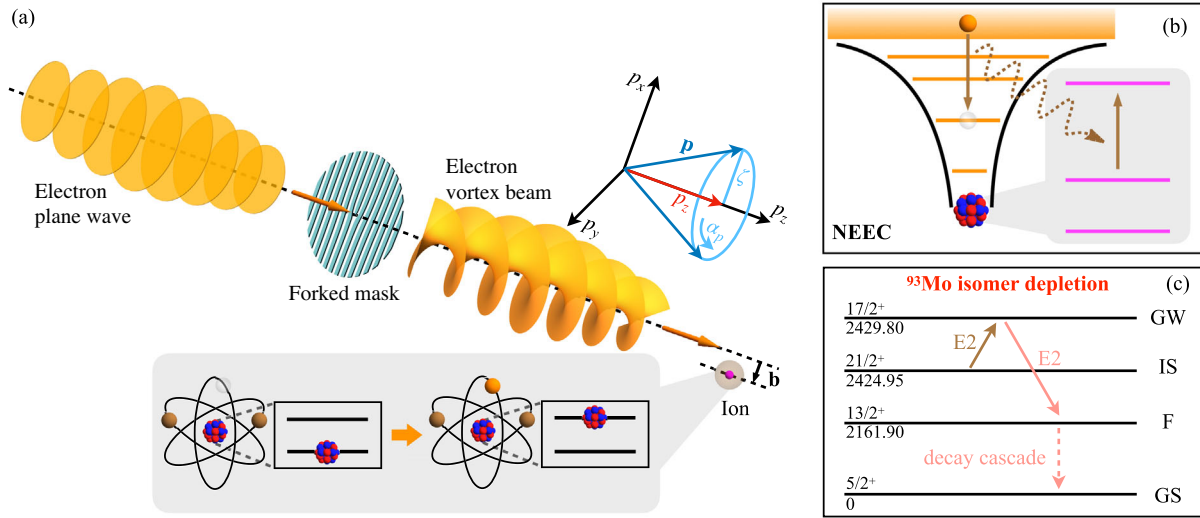
FIG. 1.   (a) A plane wave electron beam incident on a forked mask generates the electron vortex beam. Upon hitting on an ion beam with impact parameter **b**, the electrons recombine into atomic vacancies. (b) At the resonant continuum electron energy, electron recombination (orange atomic shell levels on the left) will be accompanied by nuclear excitation (magenta nuclear states on the right) in the process of NEEC. (c) Partial level scheme of ^{93}Mo. The nuclear isomeric (IS), gateway (GW), intermediate (F) and ground state (GS) levels are labeled by their spin, parity, and energy in keV [3]. The transitions IS $\rightarrow$ GW and GW $\rightarrow$ F are both of $E2$ type. Energy intervals are not to scale.

beam, the maximum effect can be shifted between capture orbitals, thus opening a route for dynamical control of isomer depletion.

In recent years, the achieved capability to fabricate phase masks with nanometer precision rendered possible to control the coherent superposition of matter waves producing typical interference patterns by spatial wave function reshaping [20–24]. Particularly interesting are vortex beams with a chiral wave function spatial profile that carry an orbital angular momentum. Optical vortices have been studied in the context of quantum communications, nanoplasmonics, and optical trapping [25,26], while imparting chirality to massive composite particles has been proposed as a method to study [27–30] and even manipulate [19,23,31,32] the inner structure of neutrons, protons, ions, and molecules. Electron vortex beams are produced by a number of techniques such as phase plates, holographic gratings, magnetic monopole fields, or chiral plasmonic near fields [20–22,27–29], with angular momenta of up to $1000\hbar$ already demonstrated. For NEEC, the nuclear transition multipolarity together with the recombination orbital impose strict selection rules on which angular momentum components of the incoming electron beam will undergo the process. While plane wave electron beams have a fixed partial wave expansion in all multipoles, vortex beams can be shaped on purpose to enhance and control the NEEC outcome.

A possible experimental implementation of this idea is depicted in Fig. 1(a). A plane wave electron beam is incident on a phase mask (for example, a forked mask), which reshapes the wave function generating an electron

vortex beam. The vortex beam is incident on ions with atomic vacancies that facilitate the NEEC process. The electron energy is chosen such as to match resonantly the nuclear transition energy upon recombination into a chosen orbital as shown in Fig. 1(b). As examples, we consider the canonical case of ^{93}Mo, whose partial level scheme is depicted in Fig. 1(c). The NEEC transition between the isomer and gateway states has 4.85 keV and electric quadrupole ($E2$) multipolarity. A second example envisaging a 19.70 keV magnetic dipole ($M1$) transition from the ^{152m}Eu isomer at 45.60 keV [3] to a gateway state will also be considered. These examples are generic and were chosen to demonstrate the effect on the two most frequently occurring nuclear transition multipolarities ($E2$ and $M1$) in the energy range relevant for NEEC. For a plane wave electron beam, the maximal NEEC cross section for depletion of ^{93m}Mo occurs for recombination into the $2p_{3/2}$ orbital of a Mo^{36+} ion [33,34]. This charge state is sufficient for providing the maximum number of vacancies in the $2p_{3/2}$ orbital. On the other hand, it ensures that the NEEC channel is allowed, with the resonance continuum electron energy of only approximately 52 eV. The resonant energy is given by the difference between nuclear transition energy and the orbital binding energy that we calculate for each specific electronic configuration using GRASP92 [35]. A higher charge state would close the NEEC channel due to the slight increase of electronic binding energies.

We consider a vortex beam with the longitudinal linear momentum p_z, the modulus of the transverse momentum $|\mathbf{p}_\perp| = \zeta$, and the topological vortex charge, a quantity

related to the electron orbital angular momentum, denoted by m [28,36]. The corresponding electron wave function can be written as

$$\psi_s(\mathbf{r}) = \int \frac{d^2\mathbf{p}_\perp}{(2\pi)^2} a_{\zeta m}(\mathbf{p}_\perp) u_{\mathbf{p}s} e^{i\mathbf{p}\cdot\mathbf{r}}, \tag{1}$$

where $a_{\zeta m}(\mathbf{p}_\perp) = (-i)^m e^{im\alpha_p} \delta(|\mathbf{p}_\perp| - \zeta)/\zeta$ and $u_{\mathbf{p}s}$ is the electron bispinor that corresponds to the plane wave solution with momentum $\mathbf{p}$ and spin state s. The linear momenta of the plane wave components are given by $\mathbf{p} = (\mathbf{p}_\perp, p_z) = (\zeta\cos\alpha_p, \zeta\sin\alpha_p, p_z)$, as sketched in Fig. 1. We choose the Oz axis parallel to the incident electron beam. To specify the lateral position of the ion with regard to the central axis of the incident electron beam, we consider an impact parameter $\mathbf{b}$ and average over the incident electron current [28,37]. The advantage of the vortex beam comes into play when restricting the impact parameter to $|\mathbf{b}| \le b$, with b chosen accordingly as a function of the incoming electron momentum [28,37]. Otherwise, an average over arbitrary impact parameters up to infinity will limit the enhancement factor for the NEEC rate to a factor p/p_z. Similar behavior is known also from the interaction of optical vortices with atomic or nuclear systems, e.g., Refs. [38–44].

The NEEC rate $Y_{\text{NEEC}}^{i\to g}$ is proportional to the modulus squared of the electron-nucleus interaction Hamiltonian matrix element $|\langle \Psi_g^N | \langle \Psi_g^e | H_N | \Psi_i^e, \psi_s \rangle | \Psi_i^N \rangle|^2$, where $|\Psi_g^e\rangle|\Psi_g^N\rangle$ is the state vector describing the total wave function of the nuclear gateway (Ψ_g^N) and electronic (Ψ_g^e) states reached by NEEC, and $|\Psi_i^e, \psi_s\rangle|\Psi_i^N\rangle$ describes the total wave function of the initial states. The total NEEC cross section can be written as a function of the continuum electron energy E,

$$\sigma_{\text{NEEC}}^{i\to g}(E) = \frac{4\pi^2}{pJ_z} Y_{\text{NEEC}}^{i\to g} \mathcal{L}(E - E_0), \tag{2}$$

where p is the modulus of the continuum electron momentum, J_z is the total incident current [36], and $\mathcal{L}(E - E_0)$ is a Lorentz profile centered on the resonance energy E_0 and with a full width at half maximum given by the width of the nuclear excited state. Typically, the nuclear widths are very narrow (for example, $\Gamma_g = 10^{-7}$ eV for the case of ^{93m}Mo), such that $\mathcal{L}(E - E_0)$ is approximated with a Dirac-deltalike profile. Integrating over the continuum electron energy, we obtain the so-called resonance strength S_v. We compare this value with the resonance strength S_p obtained for the case of a plane wave electron beam.

In order to calculate the NEEC rate $Y_{\text{NEEC}}^{i\to g}$, the vortex beam is mapped upon the partial wave expansion of the continuum electron wave function (see details in the Supplemental Material [45], which includes Ref. [46]),

$$Y_{\text{NEEC}}^{i\to g} = \frac{b^2}{4\pi} \int_0^{2\pi} \int_0^{2\pi} \frac{d\alpha_p}{2\pi} \frac{d\alpha_k}{2\pi} e^{im(\alpha_p - \alpha_k)} \mathcal{Y}_{\text{NEEC}}^{i\to g}(\mathbf{p}, \mathbf{k})$$
$$\times {}_0F_1(2; u), \tag{3}$$

with the condition $|\mathbf{p}_\perp| = |\mathbf{k}_\perp| = \zeta$ and the two polar angles α_p and α_k spanning the interval $[0, 2\pi)$. The notation ${}_0F_1$ stands for the confluent hypergeometric limit function and $u = -b^2\zeta^2[1 - \cos(\alpha_k - \alpha_p)]/2$. For a nuclear transition of multipolarity λL with $\lambda = E/M$ we have

$$\mathcal{Y}_{\text{NEEC}}^{i\to g}(\mathbf{p}, \mathbf{k}) = \frac{16\pi^3(2J_g + 1)}{(2J_i + 1)(2L + 1)^2}$$
$$\times \mathcal{B}\!\uparrow(\lambda L)\rho_i \sum_{\kappa, m_l} \frac{\mathcal{Y}_b}{2l + 1} Y_{lm_l}^*(\theta_k, \varphi_k)$$
$$\times Y_{lm_l}(\theta_p, \varphi_p), \tag{4}$$

with J_i and J_g the total angular momenta of the initial and final electronic configuration of the ion, respectively. Furthermore, $\mathcal{B}\!\uparrow(E/ML)$ is the reduced transition probability for the nuclear transition, ρ_i is the initial density of continuum electron states, and Y_{lm_l} stand for the spherical harmonics with quantum numbers l and m_l, with θ_p (θ_k) and φ_p (φ_k) as the polar and azimuthal angles of the electron momentum $\mathbf{p}$ ($\mathbf{k}$) in the spherical coordinate of the ion, respectively. For $\lambda = E$, $\mathcal{Y}_b = [C(j_g L j; \frac{1}{2}0\frac{1}{2})]^2 |R_{L,\kappa_g,\kappa}^{(E)}|^2 / R_0^{2(L+2)}$, whereas for $\lambda = M$, $\mathcal{Y}_b = (2j + 1)(\kappa_g + \kappa)^2 \times \begin{pmatrix} j_g & j & L \\ \frac{1}{2} & -\frac{1}{2} & 0 \end{pmatrix}^2 |R_{L,\kappa_g,\kappa}^{(M)}|^2 / L^2$. Here, j is the total angular momentum of the continuum electron that connects with the Dirac angular momentum quantum number κ via $j = |\kappa| - 1/2$, j_g is the total angular momentum of the bound electron in the capture orbital, and κ_g is the Dirac angular momentum quantum number of the bound electron in the capture orbital. R_0 denotes the nuclear radius. The radial integrals $R_{L,\kappa_g,\kappa}^{(E)}$ and $R_{L,\kappa_g,\kappa}^{(M)}$ for electric and magnetic multipolarities, respectively, are given in Refs. [12,47] and in the Supplemental Material [45].

We focus first on the case of ^{93m}Mo considering initially the ground state configuration of Mo^{36+} and NEEC into orbitals ranging from $2p_{3/2}$ to $4f_{7/2}$. The continuum electron resonance energy for recombination into $2p_{3/2}$ is 52 eV, while for the higher shell orbitals the values lie between 2.7 and 2.9 keV for the M shell and between 3.6 and 3.8 keV for the N shell. The vortex beam parameters are chosen such that $\zeta = p_z$ for the impact parameter range $b = 1/\zeta$. The resonance strength ratio S_v/S_p as a function of the capture orbital for three values of topological charge $m = 3, 4, 5$ is presented in Fig. 2(a). Depending on the recombination orbital, the tailored vortex electron beam leads to an enhancement between two (p orbitals) and 6 orders of magnitude (f orbitals) in the NEEC resonance
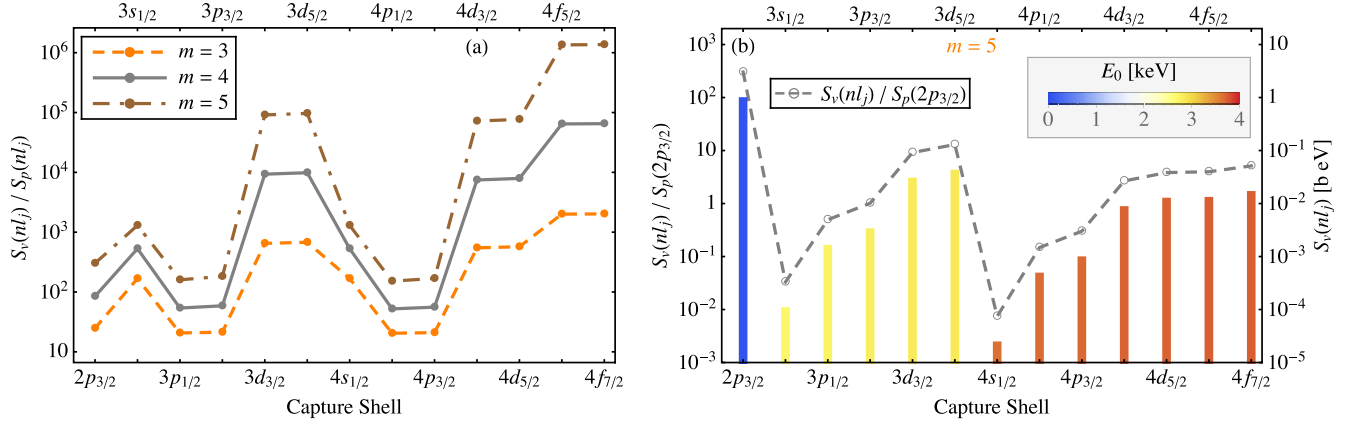
FIG. 2.   NEEC integrated cross section enhancement for the 4.85 keV nuclear transition depleting ^{93m}Mo. (a) The enhancement ratio $S_v(nl_j)/S_p(nl_j)$ comparing vortex and plane wave electron beams for recombination orbitals in the range $2p_{3/2}$–$4f_{7/2}$. (b) The ratio $S_v(nl_j)/S_p(2p_{3/2})$ of vortex beam versus maximal plane wave NEEC resonance strengths corresponding to recombination into the $2p_{3/2}$ orbital (left-hand axis, gray dashed curve with circle) and the absolute values of $S_v(nl_j)$ (right-hand axis, vertical colored bars). We consider (a) $m = 3, 4, 5$ or (b) $m = 5$, with $\zeta = p_z$ and impact parameter range $\zeta b = 1$. The resonant electron energy E_0 is presented in color coding.

strength. The physical mechanism of this enhancement is related to our choice of b. By restricting the impact parameter, we are considering the most favorable spatial region of the vortex beam, where the spherical partial wave maximizes its contribution to NEEC. This feature is missing in the case of the plane wave.

Although the enhancement for the capture into M- and N-shell orbitals is impressive, these are not the capture orbitals with the largest cross section. Provided atomic vacancies are available, NEEC into the $2p_{3/2}$ is the most efficient isomer depletion channel. We consider this value as reference for our results in Fig. 2(b) showing the vortex beam resonance strength scaled by the maximum value reached for a plane wave setup. For an incident vortex beam, the resonance strength for NEEC into this orbital is increased by 2 orders of magnitude as compared to the plane wave electron beams so far considered in the literature. In addition, also NEEC into the $3d$, $4d$, or $4f$ orbitals exceeds the plane wave value for recombination into $2p_{3/2}$ by factors ranging between 12.96 ($3d_{5/2}$) and 2.66 ($4d_{3/2}$). This might become advantageous to ease the charge state requirements or when the continuum electron energy cannot be decreased to very small energies.

NEEC angular momentum selection rules reflect upon and determine the most efficient vortex charge m for a particular NEEC process. For instance, a vortex beam with $m > 5$ would further increase NEEC into d and f orbitals. However, increasing m at values above $m = 5$ has less further enhancement effect on the NEEC resonance strength for the $2p_{3/2}$ orbitals. Depending on the envisaged electron beam energy (and, therefore, capture orbital), the proper choice of vortex beam topological charge m can maximize the NEEC resonance strength. The new aspect related to vortex beams is that m acts as a new degree of

freedom and can be dynamically controlled on an ultrafast timescale, as detailed below.

We now turn to a different example that investigates NEEC into a bare ion for a $M1$ nuclear transition in ^{152}Eu. This isotope has an isomer with 9.3 h half life lying 45.60 keV above the ground state. The envisaged μs-lived gateway state lies at 65.30 keV and has a branching ratio to the ground state [5]. Table I displays the plane wave and vortex electron beam NEEC resonance strengths for the cases of $m = 3$ and $m = 5$, assuming $\zeta = p_z$ and $\zeta b = 1$. The enhancements compared to the equivalent plane wave case are less dramatic, with factors between 1.4 and approximately 600. The lowest factor of 1.4 occurs in the case of NEEC into the $2s_{1/2}$ orbital and stems mainly from the factor p/p_z. However, the startling feature in the case of ^{152}Eu is the ability to change the most efficient capture orbital. For a $M1$ transition, the strongest NEEC resonance strength for a plane wave electron beam occurs for the recombination into the lowest available s orbital. For the specific case of ^{152}Eu, with its nuclear transition and electronic binding energies, this would be the $2s$ orbital. Surprisingly, the tailored vortex beam changes this rule of

TABLE I.   NEEC resonance strength for isomer depletion of ^{152m}Eu for both plane wave S_p and vortex S_v electron beams. We assume $\zeta = p_z$ and $\zeta b = 1$ and consider two values of the topological charge $m = 3, 5$.

nl_j	E_0 (keV)	S_p (b eV)	S_v (b eV) $m = 3$	S_v (b eV) $m = 5$
$2s_{1/2}$	5.20	8.05×10^{-4}	1.14×10^{-3}	1.14×10^{-3}
$2p_{1/2}$	5.19	7.85×10^{-5}	1.35×10^{-3}	3.34×10^{-3}
$2p_{3/2}$	6.02	1.25×10^{-5}	4.21×10^{-4}	7.61×10^{-3}

thumb, as the strongest NEEC occurs for the $2p_{1/2}$ orbital (for $m = 3$) or for the $2p_{3/2}$ orbital ($m = 5$). Thus, by manipulating the wave function of the incident electronic beam, it is possible not only to enhance rates but also to shift the maximum effect between orbitals.

In view of the many methods developed to produce specific atomic vacancies [48,49], this result can have important consequences for our ability to manipulate nuclear excitation. Vortex beam angular momentum, electron energy, and atomic vacancies can be dynamically and simultaneously controlled to optimize isomer depletion. The value of m can be switched dynamically on an ultrafast timescale by modulating the properties of plasmonic [29,50,51] and light phase masks [52,53]. Also when using physical phase plates such as the forked mask in Fig. 1, deflector coils or apertures can select the desired vortex topological charge [54]. With such dynamical control to optimize isomer depletion, clear experimental signals can be targeted, aiming at efficient nuclear energy release from isomers.

Let us now finally turn to the magnitude of isomer depletion for the ^{93m}Mo isomer. Considering the most efficient capture orbital $2p_{3/2}$ and topological charge $m = 5$, the NEEC resonance strength reaches the value ~ 1 b eV. In order to obtain a reaction rate per ion, we multiply this value by the vortex beam flux. We assume here the generic flux of 10^{24} cm^{-2} s^{-1} eV^{-1} [55,56]. The NEEC reaction rate per ion reaches the value of approximately 1 s^{-1}. Compared to the natural decay of the isomer (half life 6.8 h), this represents an enhancement of approximately 4 orders of magnitude for the isomer depletion rate. The isomers can be obtained in nuclear reactions such as ^{93}Nb$(p, n)^{93m}$Mo [4] or ^{7}Li$(^{90}$Zr$, p3n)^{93m}$Mo [6]. Since the resonance condition for electron recombination needs to be fulfilled in the rest frame of the nucleus, the ion preparation is equally important to the vortex electron beam generation. The required ion charge state breeding, storage, and cooling requires, for instance, a storage ring or an electron beam ion trap in conjunction with a radioactive beam facility. Isomeric beams have been successfully produced and stored at facilities such as the GSI Darmstadt [57–59]. At a storage ring, the condition $\zeta = p_z$ could be easily fulfilled by exploiting the Lorentz boost of the ions. The required impact parameter $b = 1/\zeta$ for this case is approximately 0.4 Å. While this should be accessible with current vortex beam focus [28,55], the spatial charge of the ion beam severely limits the number of isomers that can be addressed. A dedicated ion and electron vortex beam setup needs to be designed in order to fulfill all experimental requirements for isomer production, resonance condition match, impact parameter, and dynamical control of vortex beam properties.

Isomer depletion is a very desirable goal in view of the current search for energy storage solutions [60,61]. However, the potential of dynamically controlled vortex beams extends further than that. We anticipate new opportunities in nuclear physics, where projectile beams starting, for instance, from protons, neutrons, or muons with reshaped wave fronts [24,30] would enhance and dynamically control nuclear reactions. The beam angular momentum is ideal to specifically select reaction channels according to the final-state spin. This would enable, for instance, the targeted production of isotopes or isomers for medical applications [62,63] or the search for dark matter [64].

---

[*]yuanbin.wu@mpi-hd.mpg.de
[†]adriana.palffy-buss@physik.uni-wuerzburg.de

[1] P. Walker and G. Dracoulis, Nature (London) **399**, 35 (1999).
[2] P. Walker and Z. Podolyák, Phys. Scr. **95**, 044004 (2020).
[3] Evaluated Nuclear Structure Data Files, https://www.nndc.bnl.gov/ensdf/ (2022).
[4] J. Gunst, Y. A. Litvinov, C. H. Keitel, and A. Pálffy, Phys. Rev. Lett. **112**, 082501 (2014).
[5] A. Pálffy, J. Evers, and C. H. Keitel, Phys. Rev. Lett. **99**, 172502 (2007).
[6] C. J. Chiara, J. J. Carroll, M. P. Carpenter, J. P. Greene, D. J. Hartley, R. V. F. Janssens, G. J. Lane, J. C. Marsh, D. A. Matters, M. Polasik et al., Nature (London) **554**, 216 (2018).
[7] V. I. Goldanskii and V. A. Namiot, Phys. Lett. **62B**, 393 (1976).
[8] N. Cue, J.-C. Poizat, and J. Remillieux, Eurphys. Lett. **8**, 19 (1989).
[9] Z.-S. Yuan and J. C. Kimball, Phys. Rev. C **47**, 323 (1993).
[10] M. R. Harston and J. F. Chemin, Phys. Rev. C **59**, 2462 (1999).
[11] G. Gosselin and P. Morel, Phys. Rev. C **70**, 064603 (2004).
[12] A. Pálffy, W. Scheid, and Z. Harman, Phys. Rev. A **73**, 012715 (2006).
[13] Y. Wu, C. H. Keitel, and A. Pálffy, Phys. Rev. Lett. **122**, 212501 (2019).
[14] J. Rzadkiewicz, M. Polasik, K. Słabkowska, L. Syrocki, J. J. Carroll, and C. J. Chiara, Phys. Rev. Lett. **127**, 042501 (2021).
[15] S. Guo, Y. Fang, X. Zhou, and C. M. Petrache, Nature (London) **594**, E1 (2021).
[16] C. J. Chiara, J. J. Carroll, M. P. Carpenter, J. P. Greene, D. J. Hartley, R. V. F. Janssens, G. J. Lane, J. C. Marsh, D. A. Matters, M. Polasik et al., Nature (London) **594**, E3 (2021).
[17] Y. Wu, C. H. Keitel, and A. Pálffy, Phys. Rev. A **100**, 063420 (2019).
[18] S. Gargiulo, I. Madan, and F. Carbone, arXiv:2102.05718.
[19] I. Madan, G. M. Vanacore, S. Gargiulo, T. LaGrange, and F. Carbone, Appl. Phys. Lett. **116**, 230502 (2020).
[20] M. Uchida and A. Tonomura, Nature (London) **464**, 737 (2010).
[21] J. Verbeeck, H. Tian, and P. Schattschneider, Nature (London) **467**, 301 (2010).

[22] B. J. McMorran, A. Agrawal, I. A. Anderson, A. A. Herzing, H. J. Lezec, J. J. McClelland, and J. Unguris, Science **331,** 192 (2011).

[23] C. Clark, R. Barankov, M. Huber, M. Arif, D. G. Cory, and D. A. Pushin, Nature (London) **525,** 504 (2015).

[24] A. Luski, Y. Segev, R. David, O. Bitton, H. Nadler, A. R. Barnea, A. Gorlach, O. Cheshnovsky, I. Kaminer, and E. Narevicius, Science **373,** 1105 (2021).

[25] Y. Shen, X. Wang, Z. Xie, C. Min, X. Fu, Q. Liu, M. Gong, and X. Yuan, Light Sci. Appl. **8,** 90 (2019).

[26] K. Y. Bliokh and F. Nori, Phys. Rep. **592,** 1 (2015).

[27] S. M. Lloyd, M. Babiker, G. Thirunavukkarasu, and J. Yuan, Rev. Mod. Phys. **89,** 035004 (2017).

[28] K. Y. Bliokh, I. Ivanov, G. Guzzinati, L. Clark, R. Van Boxem, A. Béché, R. Juchtmans, M. A. Alonso, P. Schattschneider, F. Nori et al., Phys. Rep. **690,** 1 (2017).

[29] G. M. Vanacore, G. Berruto, I. Madan, E. Pomarico, P. Biagioni, R. J. Lamb, D. McGrouther, O. Reinhardt, I. Kaminer, B. Barwick et al., Nat. Mater. **18,** 573 (2019).

[30] P. Zhao, I. P. Ivanov, and P. Zhang, Phys. Rev. D **104,** 036003 (2021).

[31] H. Larocque, I. Kaminer, V. Grillo, R. W. Boyd, and E. Karimi, Nat. Phys. **14,** 1 (2018).

[32] I. Kaminer, J. Nemirovsky, M. Rechtsman, R. Bekenstein, and M. Segev, Nat. Phys. **11,** 261 (2015).

[33] Y. Wu, J. Gunst, C. H. Keitel, and A. Pálffy, Phys. Rev. Lett. **120,** 052504 (2018).

[34] J. Gunst, Y. Wu, C. H. Keitel, and A. Pálffy, Phys. Rev. E **97,** 063205 (2018).

[35] F. A. Parpia, C. F. Fischer, and I. P. Grant, Comput. Phys. Commun. **94,** 249 (1996).

[36] K. Y. Bliokh, M. R. Dennis, and F. Nori, Phys. Rev. Lett. **107,** 174802 (2011).

[37] V. Serbo, I. P. Ivanov, S. Fritzsche, D. Seipt, and A. Surzhykov, Phys. Rev. A **92,** 012705 (2015).

[38] C. T. Schmiegelow, J. Schulz, H. Kaufmann, T. Ruster, U. G. Poschinger, and F. Schmidt-Kaler, Nat. Commun. **7,** 12998 (2016).

[39] S. Franke-Arnold, Phil. Trans. R. Soc. A **375,** 20150435 (2017).

[40] A. Afanasev, C. E. Carlson, and M. Solyanik, Phys. Rev. A **97,** 023422 (2018).

[41] A. Afanasev, C. E. Carlson, C. T. Schmiegelow, J. Schulz, F. Schmidt-Kaler, and M. Solyanik, New J. Phys. **20,** 023032 (2018).

[42] S. A.-L. Schulz, S. Fritzsche, R. A. Müller, and A. Surzhykov, Phys. Rev. A **100,** 043416 (2019).

[43] A. Afanasev and C. E. Carlson, Ann. Phys. (Berlin) **2021,** 2100228 (2021).

[44] A. Afanasev, C. E. Carlson, and A. Mukherjee, Phys. Rev. Research **3,** 023097 (2021).

[45] See Supplemental Material at http://link.aps.org/supplemental/10.1103/PhysRevLett.128.162501 for the detailed NEEC rate expressions for vortex electron beams.

[46] J. Gunst, Y. Wu, N. Kumar, C. H. Keitel, and A. Pálffy, Phys. Plasmas **22,** 112706 (2015).

[47] A. Pálffy, Z. Harman, and W. Scheid, Phys. Rev. A **75,** 012709 (2007).

[48] B. Rudek, S.-K. Son, L. Foucar, S. W. Epp, B. Erk, R. Hartmann, M. Adolph, R. Andritschke, A. Aquila, N. Berrah et al., Nat. Photonics **6,** 858 (2012).

[49] M. Steck and Y. A. Litvinov, Prog. Part. Nucl. Phys. **115,** 103811 (2020).

[50] H. Kim, J. Park, S.-W. Cho, S.-Y. Lee, M. Kang, and B. Lee, Nano Lett. **10,** 529 (2010).

[51] S. Wang, C. Zhao, and X. Li, Appl. Sci. **9,** 3297 (2019).

[52] V. E. Lembessis, D. Ellinas, M. Babiker, and O. Al-Dossary, Phys. Rev. A **89,** 053616 (2014).

[53] V. E. Lembessis, Phys. Rev. A **96,** 013622 (2017).

[54] D. Pohl, S. Schneider, P. Zeiger, J. Rusz, P. Tiemeijer, S. Lazar, K. Nielsch, and B. Rellinghaus, Sci. Rep. **7,** 934 (2017).

[55] A. Béché, R. Juchtmans, and J. Verbeeck, Ultramicroscopy **178,** 12 (2017).

[56] L. Reimer and H. Kohl, Transmission Electron Microscopy (SpringerScience+Business Media, New York, 2008).

[57] Y. A. Litvinov, S. Bishop, K. Blaum, F. Bosch, C. Brandau, L. X. Chen, I. Dillmann, P. Egelhof, H. Geissel, R. E. Grisenti et al., Nucl. Instrum. Methods Phys. Res., Sect. B **317,** 603 (2013).

[58] M. Grieser, Y. A. Litvinov, R. Raabe, K. Blaum, Y. Blumenfeld, P. A. Butler, F. Wenander, P. J. Woods, M. Aliotta, A. Andreyev et al., Eur. Phys. J. Special Topics **207,** 1 (2012).

[59] T. Dickel, W. R. Plaß, S. Ayet San Andres, J. Ebert, H. Geissel, E. Haettner, C. Hornung, I. Miskun, S. Pietri, S. Purushothaman et al., Phys. Lett. B **744,** 137 (2015).

[60] R. Koningstein and D. Fork, IEEE Spectrum **51,** 30 (2014).

[61] M. Prelas, M. Matthew Boraas, F. De La Torre Aguilar, and J.-D. Seelig, Nuclear Batteries and Radioisotopes (Springer, Cham, 2016).

[62] D. Habs and U. Köster, Appl. Phys. B **103,** 501 (2011).

[63] W.-T. Pan, T. Song, H.-Y. Lan, Z.-G. Ma, J. Zhang, Z. Zhu, and W. Luo, Appl. Radiat. Isot. **168,** 109534 (2021).

[64] M. Pospelov, S. Rajendran, and H. Ramani, Phys. Rev. D **101,** 055001 (2020).